



Article

GPR and Digital Survey for the Diagnosis and the 3D Representation of the Battle of Issus Mosaic from the House of the Faun, Pompeii (Naples, Italy)

Marilena Cozzolino ^{1,*} , Antonio De Simone ², Vincenzo Gentile ¹, Paolo Mauriello ¹  and Amanda Piezzo ³

¹ Department of Agricultural, Environmental and Food Sciences, University of Molise, Via De Sanctis Snc, 86100 Campobasso, Italy; vincenzo.gentile86@gmail.com (V.G.); mauriello@unimol.it (P.M.)

² Department of Human Sciences, University Suor Orsola Benincasa, Corso Vittorio Emanuele 292, 80135 Napoli, Italy; desimone.prof@gmail.com

³ National Archaeological Museum of Naples (MANN), Ministry of Culture, Piazza Museo 19, 80135 Napoli, Italy; amanda.piezzo@beniculturali.it

* Correspondence: marilena.cozzolino@unimol.it

Abstract: The application of non-invasive geophysical techniques and digital surveys to explore cultural heritage is becoming a very important research field. The capability to detect inner and superficial changes in the inspected surfaces allows for imaging spatial inhomogeneity and material features and planning targeted conservation and restoration interventions. In this work, the results of a research project carried out on the famous Battle of Issus Mosaic, also known as the “Alexander Mosaic”, are presented. It is a masterpiece of ancient art that was found in 1831 in the House of Faun, the most luxurious and spacious house in Pompeii. It is notable for its size (3.41 × 5.82 m), the quality of workmanship and the subject that represents the culminating phase of the battle between Alexander Magno’s army and the Persian one of Darius. In 1916, it was moved inside the National Archaeological Museum of Naples, where the original horizontal location was changed with a vertical arrangement supported by an inner wooden structure, whose exact manufacture is unclear. Today, the mosaic is affected by important instability phenomena highlighted by the appearance of the significant detachment of tiles, superficial lesions and swelling of the surface. Given the important need to preserve it, a high-detail diagnostic study was realized through a digital survey and non-invasive geophysical surveys using ground-penetrating radar (GPR). The investigation was repeated after two years, in 2018 and 2020, with the aim of verifying the evolution of degradation. The work provided a high-resolution estimate of the state of the health of the mosaic and allowed for obtaining a three-dimensional reconstruction of the internal mosaic structure, including the formulation of hypotheses on the engineering supporting works of the twentieth century; this provides an essential tool for the imminent conservation project, which also implies restoring the original horizontal position.

Keywords: mosaic of alexander; GPR; digital survey; pre-conservation diagnosis



Citation: Cozzolino, M.; De Simone, A.; Gentile, V.; Mauriello, P.; Piezzo, A. GPR and Digital Survey for the Diagnosis and the 3D Representation of the Battle of Issus Mosaic from the House of the Faun, Pompeii (Naples, Italy). *Appl. Sci.* **2022**, *12*, 6965. <https://doi.org/10.3390/app12146965>

Academic Editor: Tung-Ching Su

Received: 7 June 2022

Accepted: 6 July 2022

Published: 9 July 2022

Publisher’s Note: MDPI stays neutral with regard to jurisdictional claims in published maps and institutional affiliations.



Copyright: © 2022 by the authors. Licensee MDPI, Basel, Switzerland. This article is an open access article distributed under the terms and conditions of the Creative Commons Attribution (CC BY) license (<https://creativecommons.org/licenses/by/4.0/>).

1. Introduction

In recent years, the use of non-invasive geophysical and geomatic techniques has assumed an increasingly important role in the field of cultural heritage, especially by supporting conservation and restoration projects. Geophysical methods are very useful for assessing the presence of underground structures in preventive archeology at different scales [1–6]; addressing conservation and stability issues of architectural monuments by inspecting soil foundations; assessing the mechanical properties of structural elements [7–13]; and exploring internal and superficial structures of precious and delicate targets, such as statues, wall paintings and mosaics [7,14–18]. Among these techniques, ground-penetrating radar (GPR) is widely used thanks to the miniaturization of the instrumentation, the high

investigation resolution and the minimal impact on the analyzed surfaces. For example, Masini et al. [7] presented GPR prospecting on three different constructive elements that are typical of historical buildings (a wall, a masonry pillar and a marble column), allowing for the characterization of the masonry, the detection of cracks and the imaging of metallic reinforcement bars. The obtained information was relevant for providing better knowledge of the history of the monuments and their current internal state to be evaluated for in any possible restoration intervention. Matias et al. [14] used GPR combined with seismic transmission tomography to provide important results in an investigation of columns and walls of a 14th-century UNESCO monument by giving information on the quality and spatial distribution of the materials used in the construction of the monument. Manataki et al. [15] applied different GPR systems with frequencies of 1600 MHz, 500 MHz and 250 MHz to study the mosaics of Delos island, which holds a significant body of ancient Greek art of the Hellenistic period that is on UNESCO's World Heritage List. The 1600 MHz system allowed for identifying the boundaries of the mosaic layers, as well as problematic areas, such as bulges and high levels of moisture that may cause deterioration.

For the same topics, geophysical methods can also be applied jointly with geomatic techniques that, thanks to the advances in data collection, processing and visualization, represent an important source of knowledge regarding diagnostics and documentation [19–26]. Cozzolino et al. [20] conducted a 3D metric survey through photogrammetry and ground-penetrating radar (GPR) tests applied to the study of the trapezophoros with two griffins attacking a doe of Ascoli Satriano, which is a masterpiece of ancient art that needs to be protected. The work provided information on both visible and hidden defects, such as numerous cracks that affect the sculpture. Arias et al. [21] showed the usefulness of a multidisciplinary approach to heritage documentation involving close-range photogrammetry and ground-penetrating radar techniques, as well as the development of finite-element-based structural models. The study was focused on the documentation of a medieval bridge concerning the geometric shape, the building material, and the current damage and its causes. Danese et al. [25] showed a spatial-analysis-based protocol for the interpretation of data coming from different non-invasive tests to improve the extraction process of the pattern's decay. The case study was a frescoed wall of a Gymnasium in Pompeii, which was investigated with the following non-invasive techniques: structure-from-motion photogrammetry (SfM), ground-penetrating radar and multitemporal infrared thermography. This approach enabled the extraction of decay patterns to construct a 3D model that constituted the deformation map of the painting analysis methodology and to establish the first step for the restoration of an important multilevel characterization of a fresco that is useful for the protection and mitigation of its deterioration risk.

In this study, a high-detail diagnostic investigation was realized through a digital survey and non-invasive geophysical survey using ground-penetrating radar (GPR) on the Battle of Issus Mosaic, also known as the "Alexander Mosaic". It was found on 24 October 1831 in the exedra of the peristyle of the House of the Faun (Regio VI, 12, 2) in Pompeii, which was the ancient city destroyed by the eruption of Vesuvius in 79 AD (Figures 1 and 2) [27]. In 2018, the National Archaeological Museum of Naples (MANN), where the mosaic is exposed, set up a working group, mainly composed of personnel within the institute, which is collaborating with the Central Institute for Restoration, as well as the University of Molise and the Center for Research on Archaeometry and Conservation Science (University of Naples Federico II and University of Sannio) for surveys and diagnostic investigations. The study determining the state of conservation of the mosaic was aimed at supporting the restoration project and the change of its placement. To this end, a high-detail survey was realized by the University of Molise in 2018, and it was repeated in 2020 to verify the evolution of degradation in compliance with the following workflow:

- (1) The creation of a high-resolution 3D model and orthophotos of the external surfaces through a photogrammetry digital survey in order to highlight the decay and even the type of decay, which is not perceivable by direct sight.

- (2) An analysis of the inner surfaces through the implementation of non-invasive GPR surveys with the purpose of detecting anomalies indicating voids or fractures.
- (3) An analysis of the photographic documentation produced between 1916 and 1917 in relation to the GPR data to understand the type of internal structure of support and carefully calculate its weight. This information is useful for facilitating the organization of the movement of the mosaic.
- (4) The production of new and detailed documentation, which has been non-existent so far and is useful for the imminent conservation actions.



Figure 1. Location of Pompeii on the map of Italy (a), plan of the city with the position of the House of Faun (b) and the exedra of the peristyle where the mosaic was found (c).



Figure 2. A close-up picture of the Battle of Issus Mosaic.

2. Test Site: The Battle of Issus Mosaic

The Battle of Issus Mosaic represents the triumph of Alexander the Great over Darius III of Persia in 333 BC during the Battle of Issus in Turkey. The masterpiece was created at the end of the second century BC in the opus vermiculatum technique with about 1,800,000 millimetric tesserae. In the left portion, Alexander the Great is depicted with his horse

Bucephalus. Medusa is represented on the cuirass with her wavy hair. On the right, there is Dario on a chariot as he tries to launch an assault with his men while the coachman is already whipping the horses. We also note Dario Oxyathres, who sacrifices himself to allow his brother Darius III to save himself by letting himself be pierced by the Macedonian leader. The spears, the crowding of men and horses, the fallen horse and the Persian soldier in the foreground who looks at himself in agony in a mirror bring to mind the dramatic moment of the battle.

From the moment of its discovery, there was a debate between the court, the academicians, the archaeologists, the architects and the mosaicists regarding its state of conservation and the choice of keeping it at Pompeii in its original location or detaching and transferring it to the Royal Bourbon Museum. The conservation events of the Alexander Mosaic from the House of the Faun to its current location are described in detail in [28]: “At the end, after many uncertainties, the King resolved to transfer the Mosaic in Naples and on 16 November 1843, under pouring rain, the crate containing the Mosaic of Alexander was placed on a railway wagon coming from Maddaloni, near Caserta, pulled by sixteen oxen and escorted by armed soldiers, and after a grueling journey of nine days finally came in the Royal Museum where it was exhibited, not without controversy, in the ground floor of the Gallery, in the so-called Room of the Balbi. The Mosaic remained in this place until 1916 when it was moved to the western mezzanine where Vittorio Spinazzola, Director of the National Archaeological Museum of Naples between 1910 and 1924, picked up the mosaics in a new independent collection and where it still is exposed. A detailed documentation on photographic plates, made between 1916 and 1917, is preserved in the Historical Photo Archive of Special Superintendence for the Archaeological Heritage of Naples and Pompeii. The photographs gather information relative to all phases of the moving and the final installation”. However, the type of structure created at the base of the mosaic to support it in a vertical position is not well understood as there are no shots of it.

The events briefly explained profoundly affected the state of conservation of the work, which is currently affected by important instability phenomena highlighted by the appearance of significant detachments of tiles (the occurrence is emphasized by the vibrations transmitted by car and railway traffic outside the museum), superficial lesions and swelling of the surface. In addition, it must be considered that the mosaic was designed and built to be placed on the floor, and consequently, the detachment from the site of discovery produced a significant alteration. In fact, the almost complete, albeit brief, removal of the rudus (the layer of lime, sand and aggregates, such as gravel or pebbles, which formed a concrete of consistent thickness) and the transport from the lower to the upper floor significantly affected the nucleus (the layer of mortar mixed with fragments of bricks that served as a support for the floor made of tiles). This procedure unnaturally transformed a floor mosaic into a wall mosaic [29].

3. Material and Methods

3.1. Photogrammetric Digital Survey

The production of the three-dimensional model of the mosaic surface was carried out through two photogrammetric surveys carried out in 2018 and 2020. The frames were acquired along horizontal bands (ensuring an average overlap of 80% both horizontally and vertically) at a distance of about 0.5 m from the mosaic surface using a Nikon D80 reflex camera (CCD sensor (23.6 × 15.8 mm) with 12.2 million pixels and a fixed focal length of 24 mm). The camera was set in aperture priority mode ($f/9$ value) and with an ISO sensitivity equal to 100. In order to reference the 3D model in Cartesian space in real metric units, a survey with a total station was also created using 163 clearly recognizable elements on the mosaic surface as markers. Therefore, a reference system was set up with an origin ($P = 0,0,0$) located in the lower-left corner of the mosaic and all the project data were implemented in an information system managed with Quantum GIS software (Version 3.16.11 Hannover, Open Source Geospatial Foundation, Beaverton, OR, USA).

Data processing was carried out using the Photoscan software (Agisoft Metashape Pro, Version 1.6.4, Agisoft LLC, St. Petersburg, Russia) through the following operations:

- (1) Alignment of frames using the structure-from-motion (SfM) technique [30]. Three datasets were generated: a discrete point cloud describing the object's starting geometry, the positions of the camera at the time of the acquisition of the frames and the internal calibration parameters of the camera (focal length and three radial and two tangential distortion coefficients relative to the main point).
- (2) Geometry construction through the generation of a dense cloud.
- (3) Positioning of the 3D model in Cartesian space. The points detected with the total station were entered as ground control points (GCPs) within the software. The result was the processing of a dense metric and georeferenced cloud, obtaining an average registration error of 0.007 m for the 2018 survey and 0.005 m for the 2020 survey.
- (4) Mesh generation by transforming the three-dimensional model from a point cloud to the surface of triangulated points. In order to recognize and adapt the discontinuities in the model, a "multi-resolution model" routine based on automated algorithms was used. Furthermore, an "optimization method" and a "decimation filter" were applied to reorganize and smooth the nodes of the triangles and to simplify the model and generate a multi-resolution model, respectively.
- (5) Construction of the texture through the application of digital images to the model and the creation of metric and geo-referenced orthophotos exported in the GeoTIFF format.
- (6) Generation and export in GeoTIFF format of the digital elevation model (DEM).

3.2. Ground-Penetrating Radar (GPR)

GPR is based on the diffusion of electromagnetic pulses into the soil and the recording of those re-radiated by buried targets characterized by sufficient dimensions and electromagnetic properties different from those of the surrounding ground. The quantities that are measured are the time required for the wave to travel the path from the transmitting antenna to a discontinuity and return to the surface (double time or two-way time) and the amplitude of the reflected wave. The double travel time depends on the speed with which the wave propagates within the material and provides information on the depth at which the reflectors are located. However, the amplitude, which represents how much energy returns to the surface after reflection, depends on the initial energy of the sent wave, the quantity that is dissipated along the way and the contrast of the electromagnetic properties of the materials that comprise the surface of the reflection. A complete description of the method is available in textbooks, such as [31–35].

The factors that influence the performance of the system in terms of the detectability of existing targets are the electromagnetic properties of the propagation medium, which determine the depth of investigation that can be reached, which varies from point to point. Since the attenuation of the means is a function of the radiated frequency, the use of high-frequency antennas generally allows for enhancing the resolution power, but at the expense of the penetration depth of the signals.

The georadar surveys were carried out on the entire surface of the mosaic in its actual vertical position. An IDS georadar RIS-K2 with a 3000 MHz high-resolution antenna was used for the data acquisition, whose features were considered sufficient and suitable for an overall assessment of the conservation status of the mosaic with respect to the type of target to be investigated and the thicknesses of surfaces to be analyzed.

Technically, data acquisition took place on 114 lines, from top to bottom every 5 cm, where instrumental readings were executed in continuous mode (Figure 3). In addition, several horizontal profiles and some profiles on the sides of the mosaic were acquired.



Figure 3. Grid data acquisition (a) with an IDS georadar (b).

Raw data were processed using GPR-SLICE 7.0 software (Screening Eagle Technologies Ag, Zurich, Switzerland) [36] using standard methodological approaches. In the first step, data and trace editing were executed, inserting information such as the temporal and spatial sampling intervals (time window, 20 ns; samples/scan, 512; scan/mark, 25; unit/marker, 1). Data were recorded and processed as 16-bit data and were converted by subtracting out the DC drift (wobble) in the data and, at the same time, adding a gain with time. A time-zero correction was determined to designate the starting point of the wave and the center frequency of the antenna was matched. Then, a bandpass filter and background removal were respectively applied to reduce noise from the oscillating components that had a regular frequency cycle in the frequency domain and to remove striation noises that occurred at the same time. Processed radargrams were subsequently corrected with an automatic gain control (ACG) function [37] that was applied to each trace based on the difference between the mean amplitude of the signal in the time window and the maximum amplitude of the trace. In the final step, the resulting filtered radargrams were inserted into a three-dimensional matrix from which sections were obtained at a particular double-time interval (measured in nanoseconds). Considering the complex layering and the reduced length of the profiles, we preferred to not apply the migration filter and we avoided presenting results converting time to depth using a mean value with the possibility to obtain an arbitrary and inaccurate estimate.

4. Results and Discussion

Figure 4 shows the DEMs obtained in 2018 and 2020 and Figure 5 shows some details of the last one transparently overlaid onto the processed orthophoto. The DEM analysis in 2018 (Figure 3a,b) highlighted depressions and reliefs relative to a hypothetical plane passing through the point of origin of the reference system ($P = 0,0,0$) in a spatial range of 3.66 cm. The reliefs were mainly located on the frame of the panel where the swellings responsible for the detachment of some mosaic tiles were clearly highlighted. The depressions, on the other hand, affected the central and right portions of the mosaic. The presence of an internal iron frame at the edges of the panel could, on the one hand, have favored the onset of bubbles and swelling as a consequence of the natural oxidation processes of the metal; on the other hand, it could have resisted deformations due to volumetric variations of the mortars in response to changes in temperature and humidity and/or deformations triggered by kinematic stresses (natural or artificial). This could explain the existence of depressions detected in the central part and the onset of lesions, especially on the edges (most resistant points) and the points of greatest weakness of the panel (central and right part). In order to identify the surface variations from 2018 to 2020, the point clouds of the surveys were metrically compared through the CloudCompare software (Verison 2.11 beta, Telecom ParisTech and the R&D division of EDF, Villeurbanne, France). Figure 6 shows the absolute distances between the point cloud obtained by subtracting the 2020 data from

those of 2018. On a global scale, a uniform swelling of the central part of the mosaic was estimated to be in the range of about 4 mm.

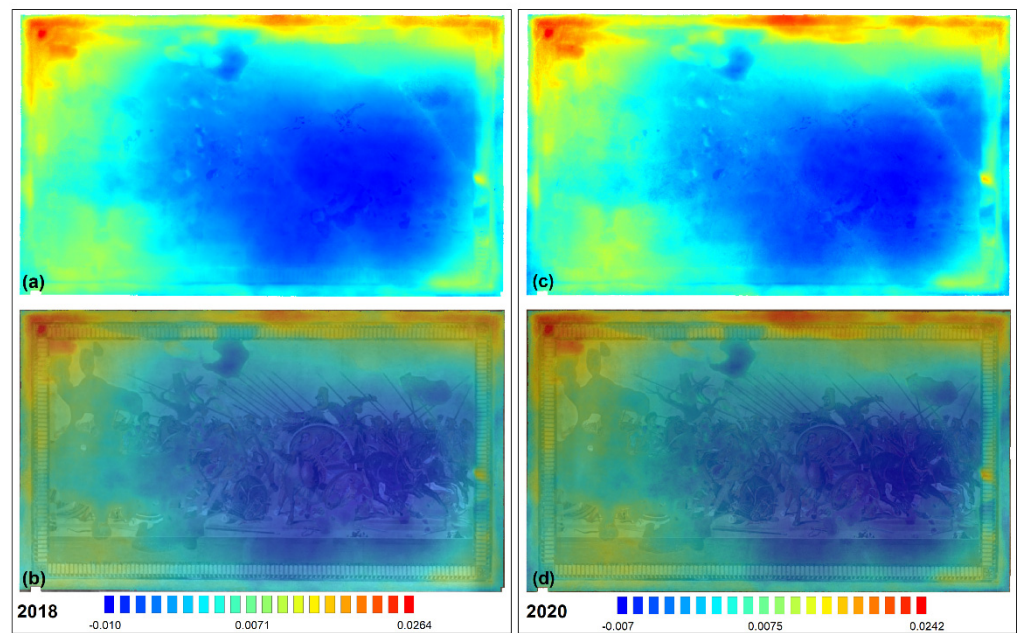


Figure 4. DEMs obtained in 2018 (a) and 2020 (c) and the same drawings transparently placed on the orthophoto (b,d). The values in the legend are expressed in meters.

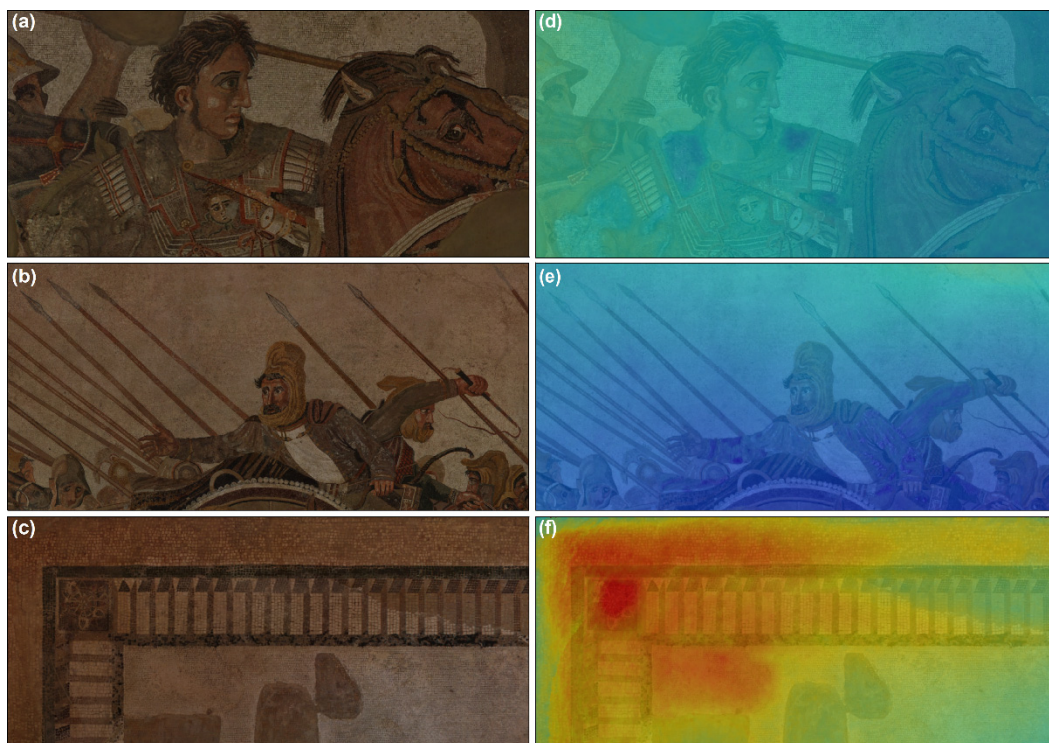


Figure 5. Details of the orthophoto obtained in 2020 (a–c) and DEMs transparently overlaid on them (d–f).

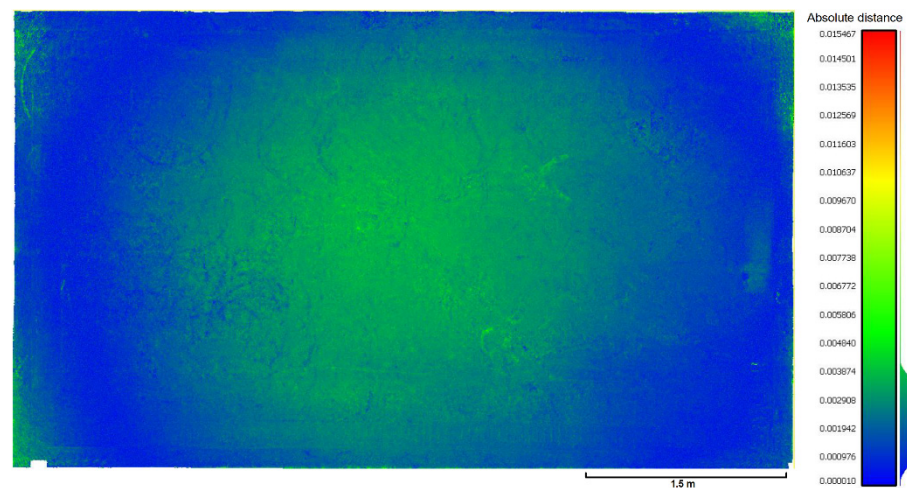


Figure 6. Absolute distance obtained by subtracting the 2020 data from 2018 data.

Figure 7 shows the images obtained in 2018 from the visual analysis of the orthophoto in which the areas affected by restorations, the detachment of tesserae and fractures are highlighted. The indication of the fractures was just quantitative and therefore they were not classified by taking into account the elevation, thickness and dimensions. The visual analysis of the orthophoto made it possible to detect in detail every single fracture and the detachment of tesserae present on the surface. The latter phenomenon, caused by multiple factors, was aggravated by the vertical position of the mosaic, which, compared with the original horizontal position, determined the displacement on the ground and the irreversible loss of the individual tiles or portions of the mosaic. The fractures had two main alignments: one vertical/horizontal, which mainly affected the edges of the mosaic, and one diagonal to the mosaic, which concerned the central/right portion of the panel. The latter was particularly relevant and fell into the areas of greatest depression recorded in the digital surface elevation model. The presence of restored and consolidated areas on the left side may have increased the resistance of the surfaces, avoiding the onset of superficial lesions.

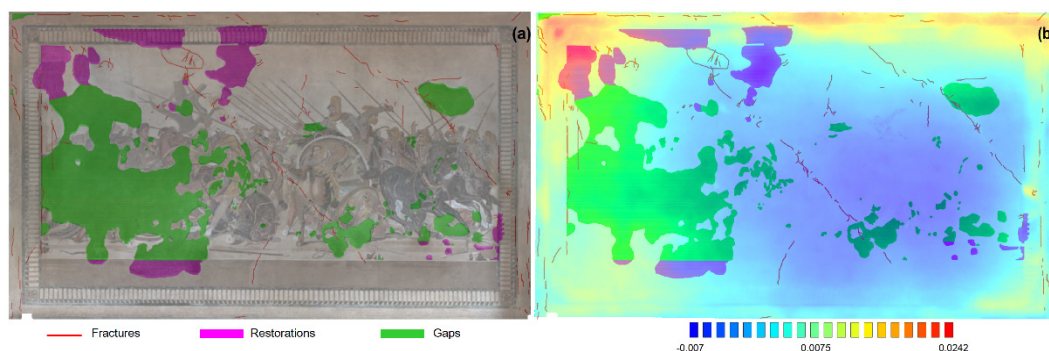


Figure 7. Restorations, detachments of tesserae and fractures reported on the orthophoto (a) and the DEM (b).

Regarding the GPR results, anomalies due to the presence of the iron support reinforcement present under the frame stood out in the different time slices (Figure 8). The degrees of amplitude variation in the time-slices were assigned a color scale that was chosen in order to show sufficient contrast to make the anomalies easily recognizable: light green corresponded to low amplitudes, while red corresponded to high amplitudes. The anomalies visible in these representations depicted the spatial distribution of the amplitudes of the reflections at specific depths within the grid. Within the sections, low amplitude variations expressed small reflections that indicated the presence of homogeneous material. High

amplitudes, on the other hand, denoted significant discontinuities in the investigated surface. In the most superficial part, we saw some anomalies of high amplitude that denoted a variation in the consistency of the materials (Figure 8b), which were located mainly on the left side of the mosaic. This aspect could be related to the presence of depressions and diagonal fractures in the central area and right side of the panel. The anomaly on the right side, near the border, was located at the point where there was swelling.

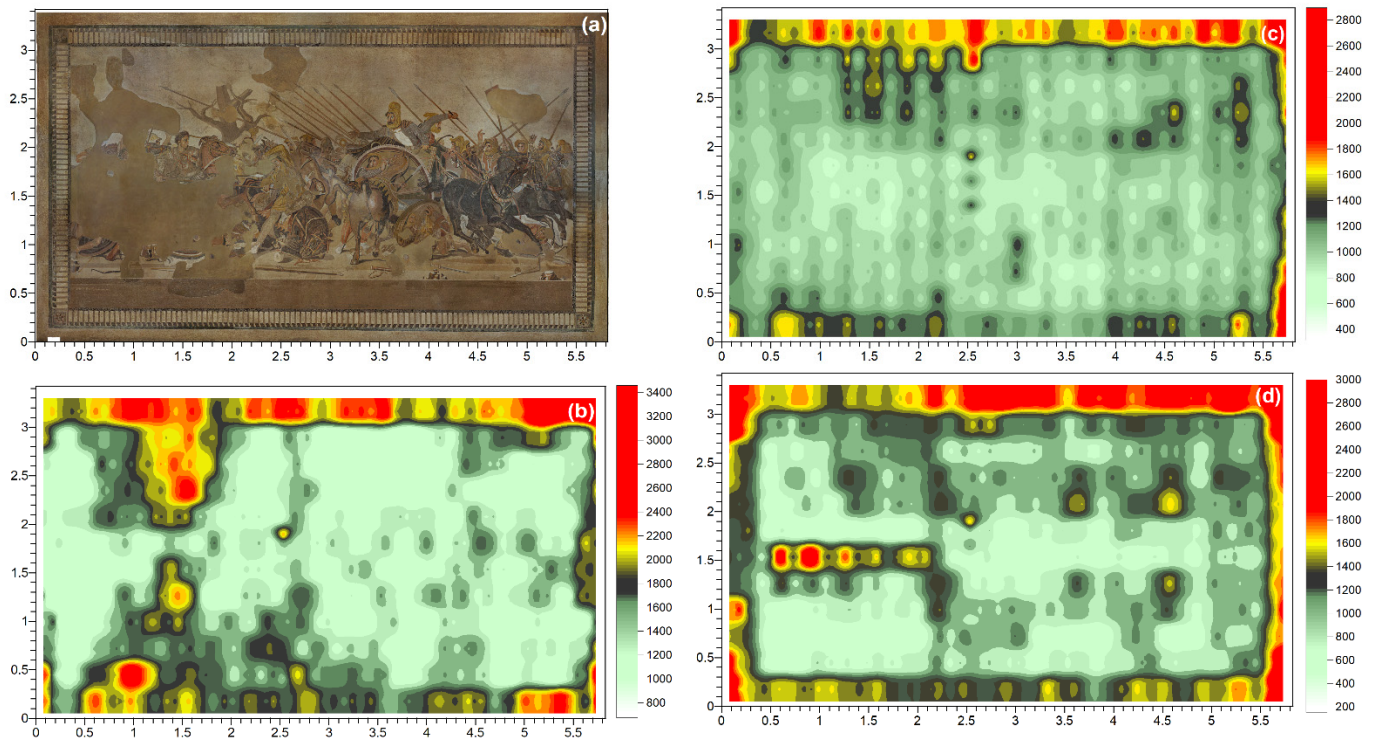


Figure 8. Details of the orthophoto obtained in 2020 (a) and slices relating to the time slices of 0.35–0.88 ns (b), 1.88–2.4 ns (c) and 3.34–3.87 ns (d).

In order to understand the inner structure, in the following part, the analysis of photographic documentation, made between 1916 and 1917, which records all phases of the moving and the final vertical installation, was jointly analyzed with GPR radargrams and slices. Following the images, it is known that the mosaic was housed on some blocks of rock. In Figure 9a, it is possible to note the original stratigraphy by recognizing, from top to bottom, the nucleus, the rudus and the screed covering the stone beams. Subsequently, the section was cleaned, the screed was removed and the stone structure was brought to light. Some wedges separated the rudus from the blocks of rock (Figure 9b). Then, the surface of the section was leveled and the rudus was cleaned of residual lime for the realization of the support frame (Figure 9c). In the next phase, equally spaced holes were drilled in the rudus, three of which are visible in Figure 9d.

From the analysis of the georadar results, it was assumed that these holes were drilled to anchor the rudus to the frame under construction by means of pins. Figure 10b shows the acquired radargram at the edge of the frame, as indicated by the green arrow on the mosaic orthophoto (Figure 10d). With red circles, the positions of the holes visible in the photos are indicated. At those points, hyperbolas are attributable to the presence of iron pins. However, there are other anomalies (indicated with yellow arrows) of the same nature. At the edges, the close hyperbolas reflected the positions of the nails used to fix the iron L-bars (blue arrows) installed in the following stages. Figure 10c shows the radargram acquired at the edge of the original frame, as indicated by the magenta arrow on the mosaic. The anomalies persisted and another one was highlighted on the left (red arrow). There were no more anomalies in the upper band. Then, the pins penetrated the mosaic by at least

15 cm (a few cm in the original one). The radargram acquired in the upper band, again at the edge of the original mosaic, highlighted the same anomalies found below (Figure 10a). Here, the pins are still visible from the top of the frame.

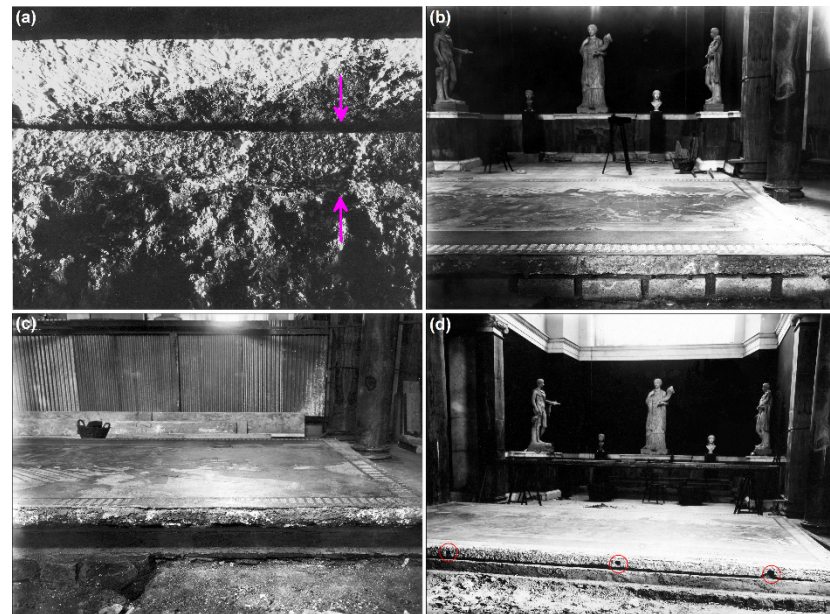


Figure 9. Photo no. 4138-1916-EX 306 (a), photo no. 4131-1916-EX 299 (b), photo no. 4129-1917-EX 297 (c) and photo no. 4130-1916-EX 298 (d).

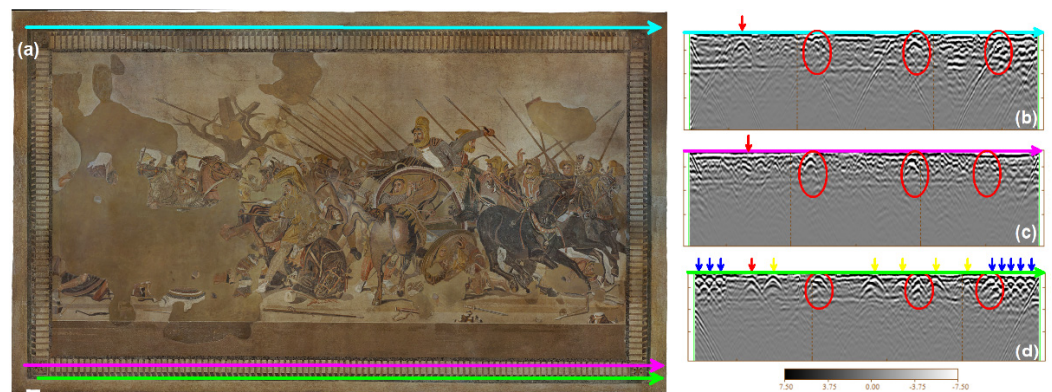


Figure 10. Location of the anchor pins (indicated by red circles) and further anomalies on three horizontal radargrams (b–d) located at the positions of the colored arrows (a).

The same situation is found on the sides where two hyperbolas are visible (Figure 11), in addition to the pins visible with the naked eye.

Figure 12 shows the digital model of the processes followed before applying the frame and removing the stone.

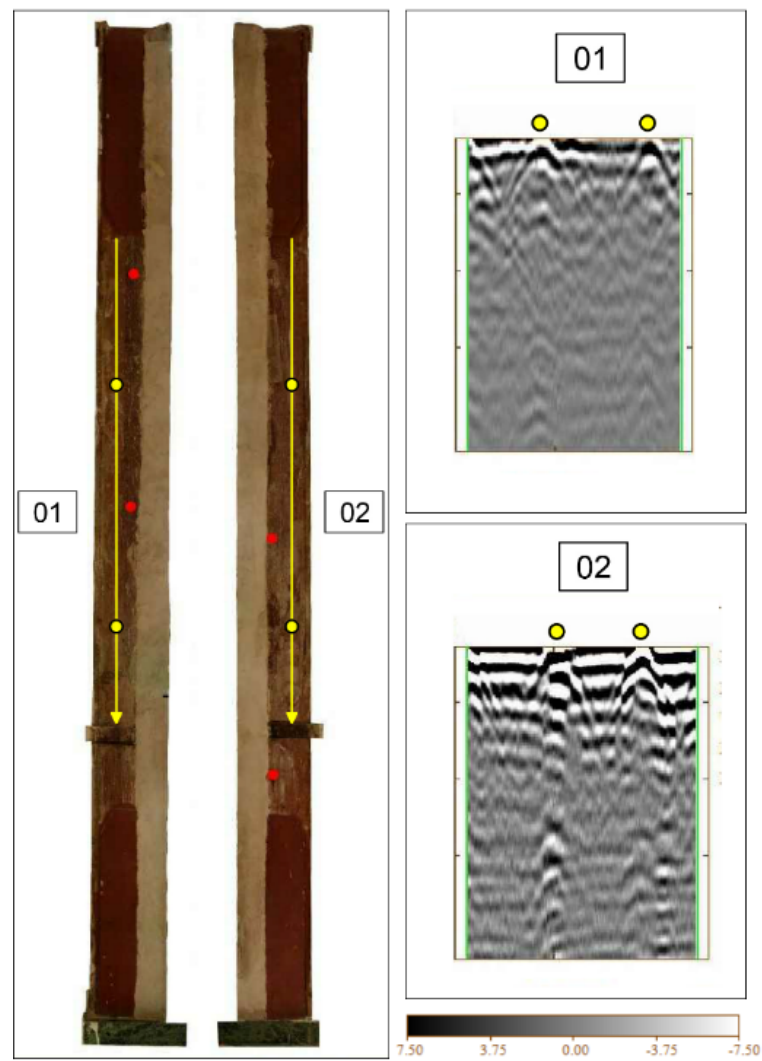


Figure 11. Orthophoto of the left and right sides of the mosaic and radargrams labeled 01 and 02. Red dots indicate visible pins.

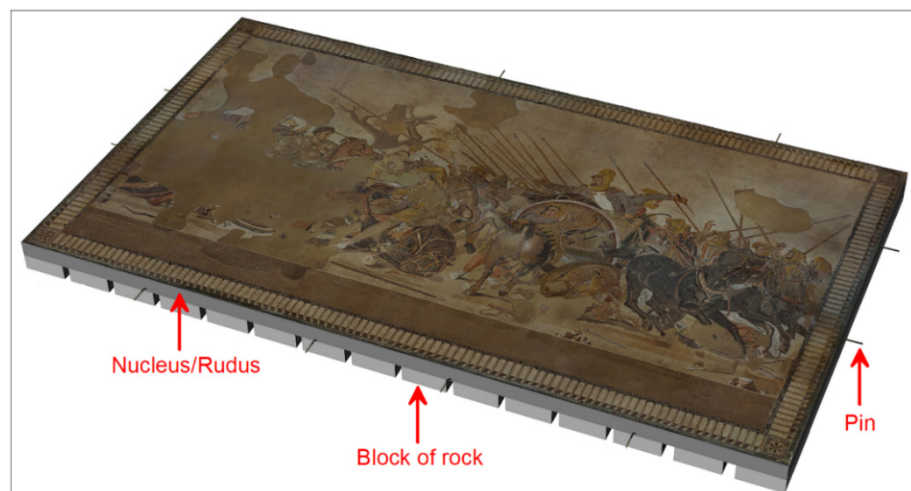


Figure 12. Digital model with the locations of the blocks of rock and the anchor pins.

The external frame was probably made using wooden crosspieces measuring 25×13 cm. Figure 13a shows a detail of Figure 9d (photo no. 4130-1916-EX 298), where in the background,

a wooden crosspiece appears with regular carvings. They were assumed to be about 10 cm wide and placed at intervals of about 22 cm. Figure 13b shows the digital model of the carved frame. It was assumed that this element is related to the underlying part of the longitudinal crosspiece that was specially prepared to house the elements of the internal filling.

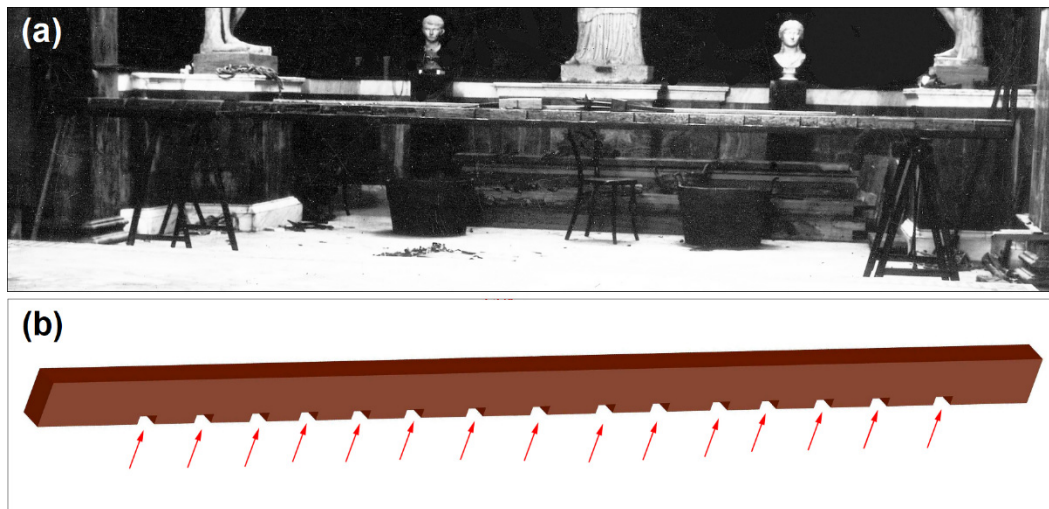


Figure 13. Photo no. 4130-1916-EX 298 (a) and digital model of the frame with indication of the notches using red arrows (b).

The anchoring of the wooden crosspieces with the mosaic is described in the previous section. To reinforce the structure, four angular iron bars were added (Figure 14). Holes were also drilled to position the protective covering of the front part of the mosaic. A 2 cm board was placed under the wooden crosspieces, which were placed under the stone crosspieces (Figure 14a). This table was probably removed in the next phases.

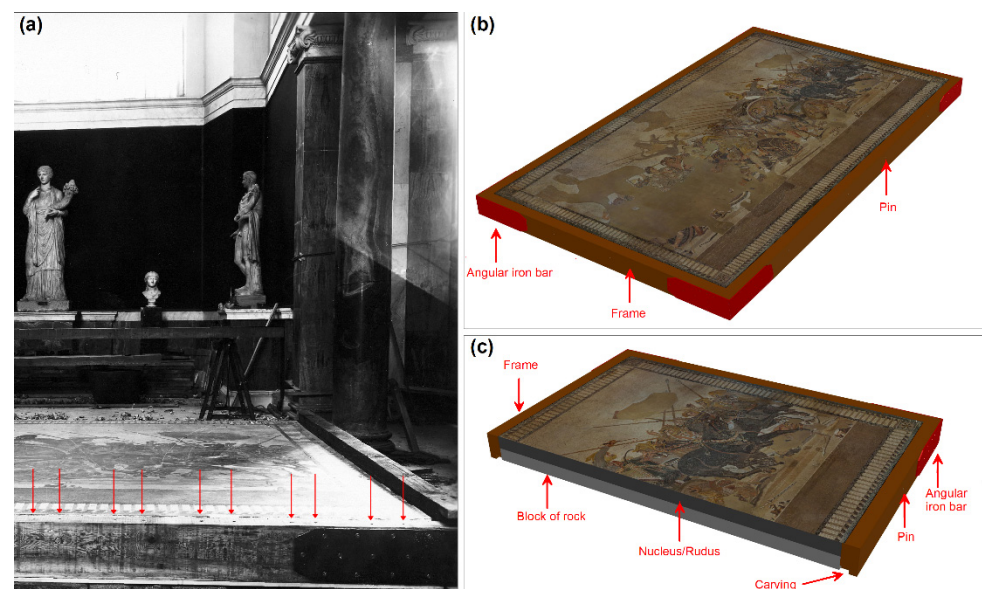


Figure 14. Photo no. 4132-1916-EX 300 (a), a digital model with the anchoring of the frame and addition of iron angles (b) and a cross-section (c).

A protective sheet was added to the surface, which was blocked with a board on the edge by means of nails in the pre-drilled points in the previous step (Figure 15a). Some sides were added (10 cm wide and 5 cm high) in between where the wide boards were to be placed (Figure 15b). The gaps were subsequently sealed with mortar (Figure 15c). After

which, the lifting of the recessed mosaic began (Figure 14d), which was placed in a vertical position on a support (Figure 15e).

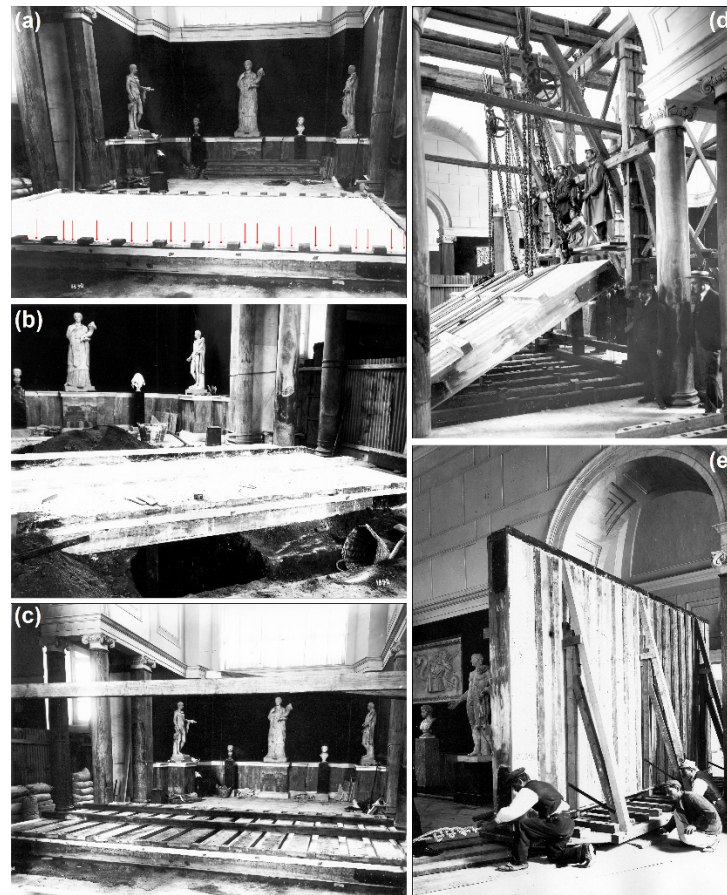


Figure 15. Photo no. 4133-1916-EX 301 (a), photo no. 4134-1916-EX 302 (b), photo no. 4135-1916-EX 303 (c), photo no. 4157-1917-EX 325 (d) and photo no. 4173-1917-EX 341 (e).

On the back, from a historical photo, an alternation of narrow dark boards and wide light boards, 10 cm and 22 cm wide, respectively, can be noted (Figure 16a). In the GPR slice relating to the time window 1.88–2.4 ns (Figures 8b and 16b), a series of vertical anomalies were highlighted that began directly in contact with the rudus. It was plausible that the wooden structure placed at the rear of the mosaic traced this structure in some way. In particular, it is likely that the narrow boards were actually beams or murals 10 cm wide (with a maximum length of 14 cm, depending on the thickness of the shaving made under the rudus), which rested directly under the mosaic. As can be seen from many of the radargrams, some profiles seemed to be characterized by the presence of metal elements as brackets to block the vertical wooden beams from the rudus. An example is shown in Figure 17, where three identifiable hyperbolas emerged clearly with the rudus, the filling lime and the closing table. Hyperbolas 1 and 2 (Figure 17a) often penetrated the mosaic and probably represented a system for anchoring the possible wooden beam (vertical georadar anomalies) directly to the mosaic. At approximately hyperbola 3, a sort of reinforcement was evident under the vertical structures (Figure 18). The spaces were probably filled with plaster and closed everything with the boards that were visible on the back. The slice (Figure 17b), which was related to the time window between 3.34 ns and 3.87 ns, was enhanced to visualize the three anomalies jointly, even if detected at different depths.

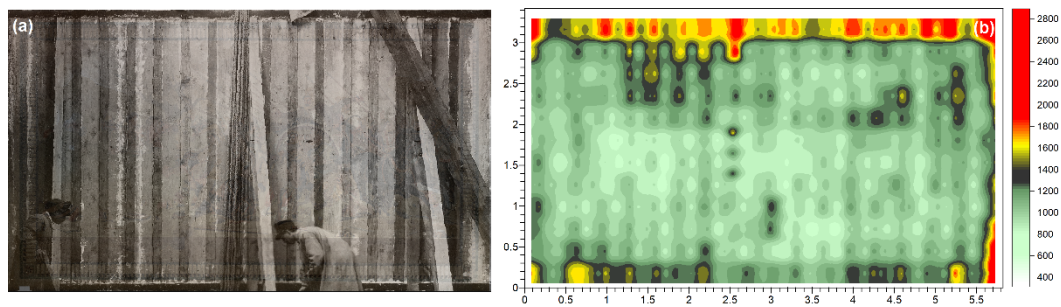


Figure 16. Historical photo (photo no. 4172-1917-EX 340) straightened and positioned on the back of the mosaic (a) and time slice relating to the time window 1.88–2.4 ns (b).

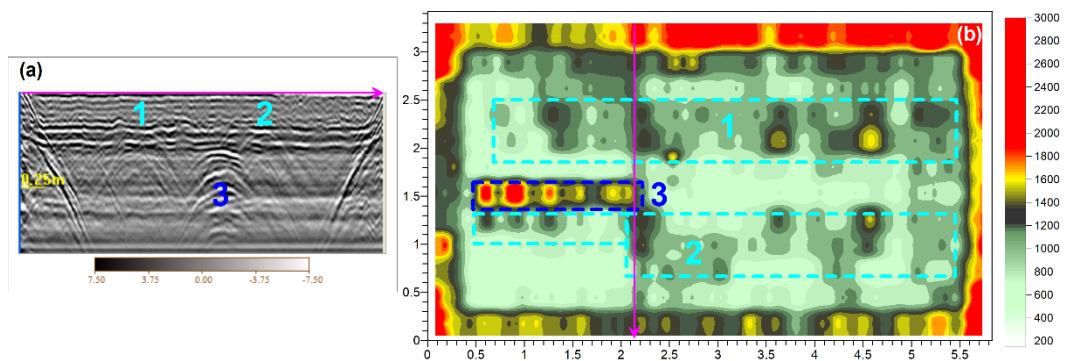


Figure 17. Main anomalies, labeled 1, 2 and 3, indicated on the radargram (acquired as indicated by the magenta arrow) (a) and on the slice relating to the time window 3.34–3.87 ns (b).

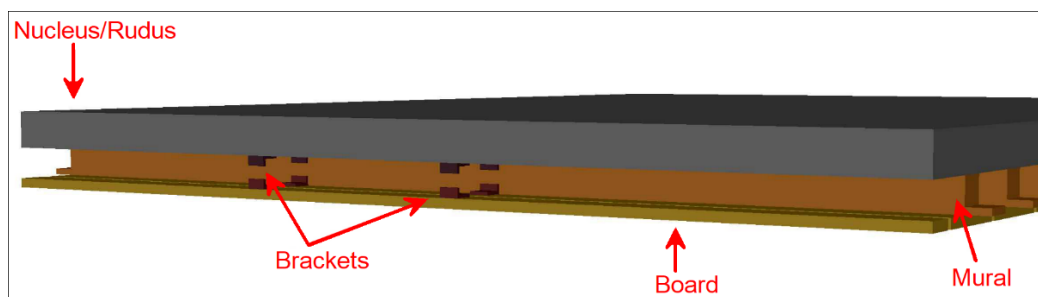


Figure 18. Anchor system digital model.

Therefore, after the removal of the blocks of rock, the vertical beams would have been housed (directly or indirectly) thanks to the notches located at the base of the longitudinal beams of the frame. In this system, it is possible to make four hypotheses based on the presumed depth of the notch, the location of the vertical beams and the closing plank. The hypotheses in question took into account the position and shape of the acquired georadar anomalies:

Hypothesis 1. (Figure 19): Support boards (25 × 12 cm) were inserted at regular intervals under the rudus. The boards were closed in the lower part with boards (10 × 2 cm) that protrude by 2 cm outside. The empty space between the support boards was filled with plaster. We consider this hypothesis the least probable, as it does not explain the presence of the georadar anomalies previously discussed.

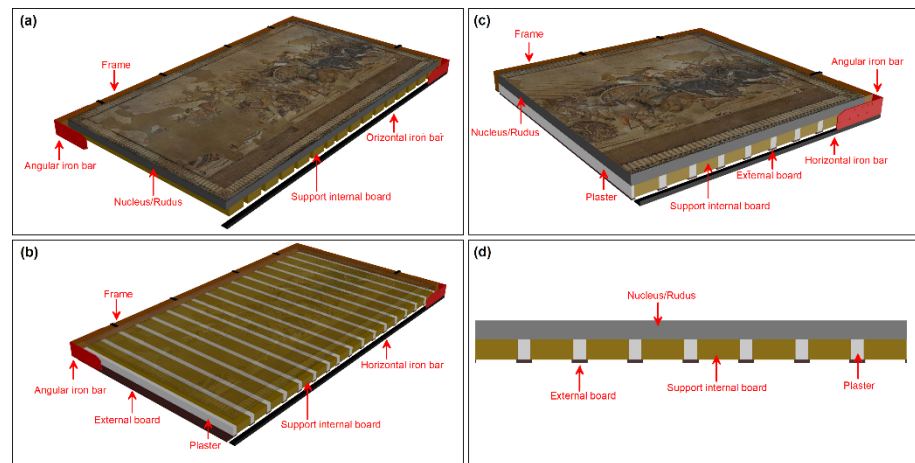


Figure 19. Hypothesis 1 digital model: locations of support boards under the rudus (a), complete support system (b), cross-section (c) and longitudinal section (d).

Hypothesis 2. (Figure 20): The vertical beams inserted at regular intervals were worked to be housed and nailed to the frame. Between one beam and the other, closing tables were inserted through brackets. The gaps left empty between the beams were filled with plaster.

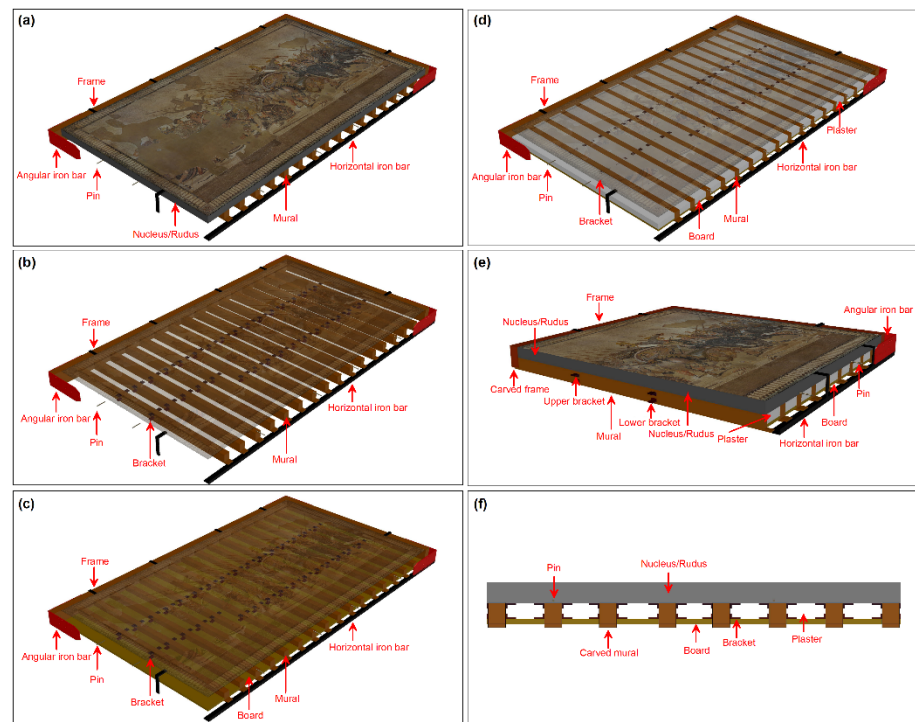


Figure 20. Hypothesis 2: locations of vertical beams (a), locations of anchoring brackets (b), locations of closing boards (c), complete support system (d), cross-section (e) and longitudinal section (f).

Hypothesis 3. (Figure 21): This differs from hypothesis 2 in that the incision was made to be 12 cm in order to completely contain the vertical beam that rests directly under the rudus and protrudes 2 cm outside.

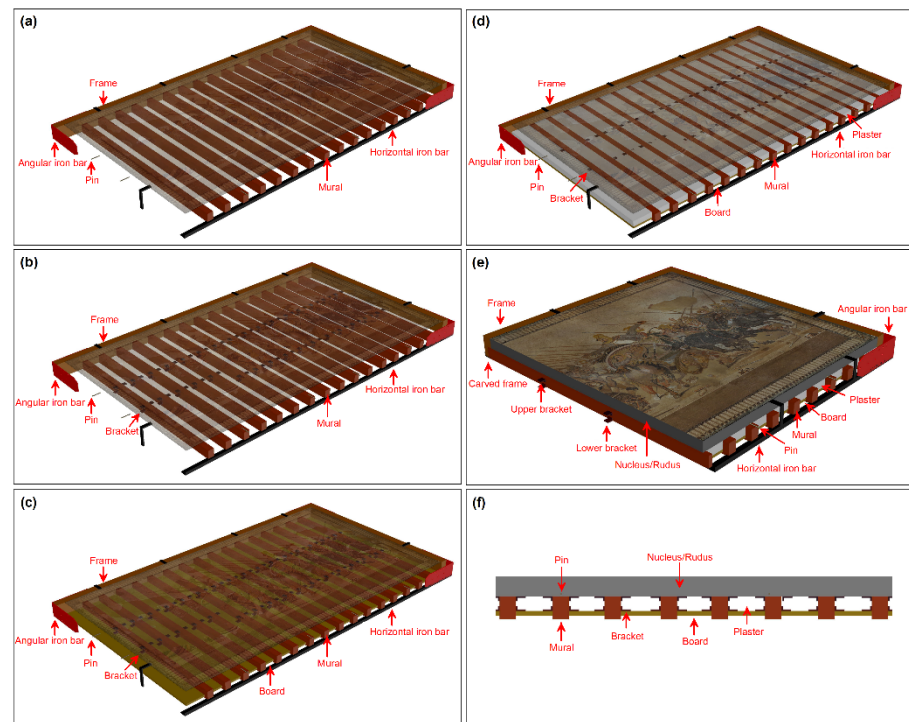


Figure 21. Hypothesis 3 digital model: positions of vertical beams (a), locations of anchoring brackets (b), arrangement of closing tables (c), complete support system (d), cross-section (e) and longitudinal section (f).

Hypothesis 4. (Figure 22): The planks were anchored to the vertical beams by means of brackets according to a “T” system. Closing tables were inserted between one plank and the other. The gaps left empty between the beams were filled with plaster. This is the hypothesis that best matches the shape and position of the georadar anomalies.

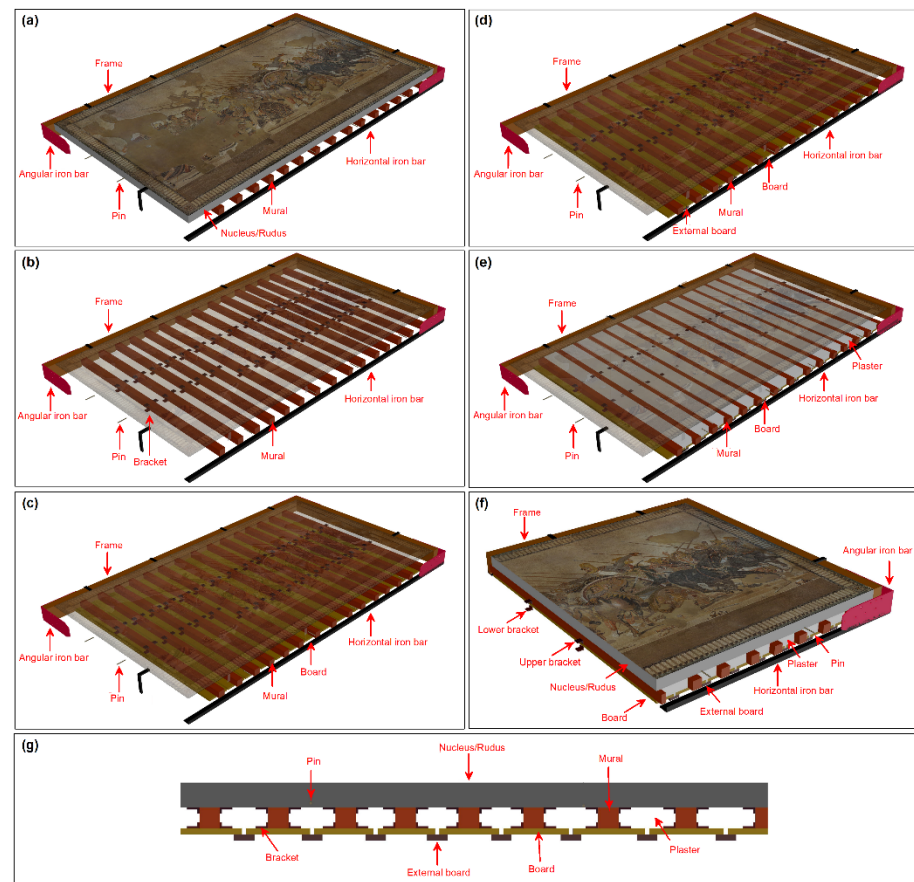


Figure 22. Hypothesis 4 digital model: vertical beam positions (a), anchoring bracket locations (b), board arrangements (c), external board positions (d), complete support system (e), cross-section (f) and longitudinal section (g).

5. Conclusions

In this study, the issue connected to the conservation of the Alexander Mosaic was investigated in an organic and exhaustive way, starting from the analysis of the available knowledge framework. From an operational point of view, the adopted research methodology provided for the recognition of all available documentation, an accurate survey of the current state from the morphological point of view and non-invasive diagnostic investigations. This allowed for obtaining a further preliminary and in-depth knowledge phase of the asset to also provide a framework for comparison with what emerged from previous studies and, therefore, data on any changes in the state of conservation of the asset. In detail, in addition to a slight progression of the degradation phenomena already recorded in 2018, regarding the lesions, anomalies in the support emerged from the diagnostic results, which suggested the presence of discontinuities in the background mortar. This could have probably been due to the presence of different materials, with particular reference to the mosaic embedding system put in place during the transfer in 1916, consisting of a wooden frame placed along the perimeter, with interposed wooden joists reinforced with metal elements. However, to date, insufficiently exhaustive data has emerged regarding the state of conservation of the support that is not visible and cannot be inspected directly and the actual state will be fully detected only after moving the mosaic from its current position, making the back accessible. Currently, the first phase of the restoration can now be considered completed, which was limited to interventions to make the mosaic surface safe, which was necessary in the face of the detected degradation phenomena and limited only to the elimination of the conditions that can generate critical issues during movement (loose tiles, presence of continuity solutions between the layers, etc.). Subsequently, the mosaic will be overturned, following which it will be possible to access the support to

promptly check its conservation status, fine-tune the subsequent conservation interventions and possibly provide for the construction of a new collection system should the existing one prove to be no longer suitable. Subsequently, the mosaic will be placed in a horizontal position that will allow for the restoration of the mosaic surface and the final rearrangement to be carried out. The restoration operations, which will also affect the rear parts, will be preceded by further diagnostic analyzes once the mosaic is overturned. In this way, at the end of the project, a complete model will be obtained, which will integrate all the results and will represent a precious source of knowledge on this important artifact.

Author Contributions: Conceptualization, M.C., P.M., A.D.S. and A.P.; Data curation, M.C., P.M. and V.G.; Methodology M.C., P.M. and V.G.; Validation, M.C., P.M., A.D.S., A.P. and V.G.; Writing—original draft, M.C., P.M. and V.G.; Writing—review and editing, M.C., P.M. and V.G. All authors have read and agreed to the published version of the manuscript.

Funding: This research received no external funding.

Institutional Review Board Statement: Not applicable.

Informed Consent Statement: Not applicable.

Acknowledgments: Special thanks to Paolo Giulierini for having involved us in this important project and for having been a constant guide, always demonstrating the greatest passion and dedication to the protection of this very important masterpiece. We are also very thankful to the company “Boviar. Integrated systems for diagnostics and monitoring”, in particular Filippo Bovio, for the technical-scientific support during the data acquisition and processing phases.

Conflicts of Interest: The authors declare no conflict of interest.

References

1. Cozzolino, M.; Bakovic, M.; Borovinic, N.; Galli, G.; Gentile, V.; Jabucanin, M.; Mauriello, P.; Merola, P.; Živanovic, M. The Contribution of Geophysics to the Knowledge of the Hidden Archaeological Heritage of Montenegro. *Geosciences* **2020**, *10*, 187. [[CrossRef](#)]
2. Fassbinder, J.W.E.; Reindel, M. Magnetometer prospection as research for pre-Spanish cultures at Nasca and Palpa, Perú. In Proceedings of the 6th International Archaeological Prospection Conference, Rome, Italy, 14–17 September 2005; Piro, S., Ed.; CNR: Roma, Italy, 2005; pp. 6–10.
3. Tsokas, G.N.; Giannopoulos, A.; Tsourlos, P.; Vargemezis, G.; Tealby, J.M.; Sarris, A.; Papazachos, C.B.; Savopoulou, T. A large scale geophysical survey in the archaeological site of Europos (northern Greece). *J. Appl. Geophys.* **1994**, *32*, 85–98. [[CrossRef](#)]
4. Papadopoulos, N.G.; Tsourlos, P.; Tsokas, G.N.; Sarris, A. Two-dimensional and three-dimensional resistivity imaging in archaeological site investigation. *Archaeol. Prospect.* **2006**, *13*, 163–181. [[CrossRef](#)]
5. Cozzolino, M.; Calì, L.M.; Gentile, V.; Mauriello, P.; Di Meo, A. The Discovery of the Theater of Akragas (Valley of Temples, Agrigento, Italy): An Archaeological Confirmation of the Supposed Buried Structures from a Geophysical Survey. *Geosciences* **2020**, *10*, 161. [[CrossRef](#)]
6. Cozzolino, M.; Gentile, V.; Giordano, C.; Mauriello, P. Imaging Buried Archaeological Features through Ground Penetrating Radar: The Case of the Ancient Saepinum (Campobasso, Italy). *Geosciences* **2020**, *10*, 225. [[CrossRef](#)]
7. Masini, N.; Persico, R.; Rizzo, E. Some examples of GPR prospecting for monitoring of the monumental heritage. *J. Geophys. Eng.* **2010**, *7*, 190–199. [[CrossRef](#)]
8. Tsourlos, P.I.; Tsokas, G.N. Non-destructive electrical resistivity tomography survey at the south walls of the Acropolis of Athens. *Archaeol. Prospect.* **2011**, *18*, 173–186. [[CrossRef](#)]
9. Catapano, I.; Ludeno, G.; Soldovieri, F.; Tosti, F.; Padeletti, G. Structural assessment via ground penetrating radar at the Consoli Palace of Gubbio (Italy). *Remote Sens.* **2018**, *10*, 45. [[CrossRef](#)]
10. Pirinu, A.; Balia, R.; Piroddi, L.; Trogu, A.; Utzeri, M.; Vignoli, G. Deepening the knowledge of military architecture in an urban context through digital representations integrated with geophysical surveys. The city walls of Cagliari (Italy). In Proceedings of the 2018 IEEE International Workshop on Metrology for Archaeology and Cultural Heritage, Cassino, Italy, 22–24 October 2018; pp. 211–215.
11. Angelis, D.; Tsourlos, P.; Tsokas, G.; Vargemezis, G.; Zacharopoulou, G.; Power, C. Combined application of GPR and ERT for the assessment of a wall structure at the Heptapyrgion fortress (Thessaloniki, Greece). *Appl. Geophys.* **2018**, *152*, 208–220. [[CrossRef](#)]
12. Pérez-Gracia, V.; Caselles, J.O.; Clapes, J.; Osorio, R.; Martínez, G.; Canas, J.A. Integrated near-surface geophysical survey of the Cathedral of Mallorca. *J. Archaeol. Sci.* **2009**, *36*, 1289–1299. [[CrossRef](#)]
13. Cozzolino, M.; Gentile, V.; Mauriello, P.; Peditrou, A. Non-Destructive Techniques for Building Evaluation in Urban Areas: The Case Study of the Redesigning Project of Eleftheria Square (Nicosia, Cyprus). *Appl. Sci.* **2020**, *10*, 4296. [[CrossRef](#)]

14. Matias, M.; Almeida, F.; Moura, R.; Barraca, N. High resolution NDT in the characterization of the inner structure and materials of heritage buildings walls and columns. *Constr. Build. Mater.* **2021**, *267*, 121726. [CrossRef]
15. Manataki, M.; Maris, C.; Sarris, A.; Vafidis, A. Using GPR to Evaluate the Stratigraphic Condition of the Mosaic of the Dolphins in Delos Island, Greece, in order to Adopt the necessary Conservation measures. In Proceedings of the 10th International Workshop on Advanced Ground Penetrating Radar, The Hague, The Netherlands, 9–11 September 2019; pp. 1–7.
16. Piroddi, L.; Vignoli, G.; Trogu, A.; Deidda, G.P. Non-destructive Diagnostics of Architectonic Elements in San Giuseppe Calasanzio's Church in Cagliari: A Test-case for Micro-geophysical Methods within the Framework of Holistic/integrated Protocols for Artefact Knowledge. In Proceedings of the 2018 IEEE International Conference on Metrology for Archaeology and Cultural Heritage, Cassino, Italy, 22–24 October 2018; pp. 17–21.
17. Urban, T.M.; Bennett, M.R.; Bustos, D.; Manning, S.W.; Reynolds, S.C.; Belvedere, M.; Odess, D.; Santucci, V.L. 3-D radar imaging unlocks the untapped behavioral and biomechanical archive of Pleistocene ghost tracks. *Sci. Rep.* **2019**, *9*, 16470. [CrossRef] [PubMed]
18. Wiewel, A.; Conyers, L.; Piroddi, L.; Papadopoulos, N. An Experimental Use of Ground-Penetrating Radar to Identify Human Footprints. *ArcheoSciences* **2021**, *45*, 143–146. [CrossRef]
19. Donadio, E.; Spanò, A.; Sambuelli, L.; Picchi, D. Three-Dimensional (3D) modelling and optimization for multipurpose analysis and representation of ancient statues. In *Latest Developments in Reality-Based 3D Surveying and Modelling*; Remondino, F., Georgopoulos, A., Gonzalez-Aguilera, D., Agrafiotis, P., Eds.; MDPI: Basel, Switzerland, 2018; pp. 95–118. ISBN 978-3-03842-684-4.
20. Cozzolino, M.; Di Meo, A.; Gentile, V.; Mauriello, P.; Zullo, E. Combined Use of 3D Metric Survey and GPR for the Diagnosis of the Trapezophoros with Two Griffins Attacking a Doe of Ascoli Satriano (Foggia, Italy). *Geosciences* **2020**, *10*, 307. [CrossRef]
21. Arias, P.; Armesto, J.; Di-Capua, D.; González-Drigo, R.; Lorenzo, H.; Pérez-Gracia, V. Digital photogrammetry, GPR and computational analysis of structural damages in a mediaeval bridge. *Eng. Fail. Anal.* **2007**, *14*, 1444–1457. [CrossRef]
22. Oses, N.; Dornaika, F.; Moujahid, A. Image-based delineation and classification of built heritage masonry. *Remote Sens.* **2014**, *6*, 1863–1889. [CrossRef]
23. Costanzo, A.; Minasi, M.; Casula, G.; Musacchio, M.; Buongiorno, M.F. Combined use of terrestrial laser scanning and IR thermography applied to a historical building. *Sensor* **2015**, *15*, 194–213. [CrossRef] [PubMed]
24. Barrile, V.; Bilotta, G.; Meduri, G.M.; De Carlo, D.; Nunnari, A. Laser Scanner technology, ground-penetrating radar and augmented reality for the survey and recovery of the artistic, archaeological and cultural heritage. *ISPRS Ann. Photogramm. Remote Sens. Spat. Inf. Sci.* **2017**, *4*, 123–127. [CrossRef]
25. Danese, M.; Sileo, M.; Masini, M. Geophysical Methods and Spatial Information for the Analysis of Decay frescoes. *Surv. Geophys.* **2018**, *39*, 1149–1166. [CrossRef]
26. Cozzolino, M.; Gabrielli, R.; Galatà, P.; Gentile, V.; Greco, G.; Scopinaro, E. Combined use of 3D metric surveys and non-invasive geophysical surveys for the determination of the state of conservation of the Stylite Tower (Umm ar-Rasas, Jordan). *Ann. Geophys.* **2019**, *61*, 72. [CrossRef]
27. Bonucci, C. Scavi romani di Pompei, Ercolano, Boscotrecase, luglio a dicembre. *BullInst* **1832**, *1*, 11.
28. Melillo, L. Das Alexandermosaik aus der Casa del Fauno in Pompeji—Die fruhen Bergungsmassnahmen. In *Alexander der Grosse und die Oeffnung der Welt Asiens Kulturen im Wandel*, 1st ed.; Hansen, S., Wiczorek, A., Tellenbach, M., Eds.; Schnell & Steiner: Mannheim, Germany, 2009; pp. 61–65. ISBN 978-3795421779.
29. De Simone, A.; Piezzo, A. Il restauro del mosaico di Alessandro tra immagine e materia: Ultimi studi e prime ipotesi di intervento. In *Atti del XXVII Colloquio Dell'associazione Italiana per lo Studio e la Conservazione del Mosaico*, 27th ed.; Angelelli, C., Erba, M.E., Massara, D., Zulini, E., Eds.; Quasar: Rome, Italy, 2022; pp. 5–10. ISBN 987-88-5491-248-9.
30. Remondino, F.; El-Hakim, S. Image-based 3-D modelling: A review. *Photogramm. Rec.* **2006**, *21*, 269–291. [CrossRef]
31. Conyers, L.B. *Interpreting Ground-Penetrating Radar for Archaeology*; Left Coast Press: Walnut Creek, CA, USA, 2012.
32. Everett, M.E. *Near-Surface Applied Geophysics*; Cambridge University Press: Cambridge, UK, 2013.
33. Goodman, D.; Piro, S. *GPR Remote Sensing in Archaeology*; Springer: Berlin/Heidelberg, Germany, 2013.
34. Reynolds, J.M. *An Introduction to Applied and Environmental Geophysics*, 2nd ed.; John Wiley & Sons: Oxford, UK, 2011.
35. Cozzolino, M.; Di Giovanni, E.; Mauriello, P.; Piro, S.; Zamuner, D. *Geophysical Methods for Cultural Heritage Management*; Geophysics Series; Springer: Cham, Switzerland, 2018.
36. GPR-SLICE Software. Available online: <http://www.gprsurvey.com/practice/GPR-SLICE> (accessed on 13 May 2022).
37. Jol, H. *Ground Penetrating Radar: Theory and Applications*; Elsevier: Amsterdam, The Netherlands, 2009; ISBN 978-0-444-53348-7.